Miyazawa *Earth, Planets and Space* (2016) 68:205
DOI 10.1186/s40623-016-0585-z

Earth, Planets and Space

LETTER Open Access

An investigation into the remote triggering of the Oita earthquake by the 2016 Mw 7.0 Kumamoto earthquake using full wavefield simulation

Masatoshi Miyazawa*

Abstract

High-amplitude seismic waves from the Mw 7.0 Kumamoto earthquake of April 16, 2016, triggered another large earthquake 80 km to the NE roughly 30 s later. The source was located at shallow depths beneath the Yufuin geothermal field, Oita Prefecture, Japan, and the event magnitude was approximately 5.9. To date, this is one of the clearest known examples of a remotely triggered large earthquake. The triggered Oita event was followed by significant seismicity, which was distinct from the aftershocks of the Kumamoto earthquake. The Coulomb failure stress change around the hypocenter, calculated for the passing waves of the Kumamoto earthquake by full wavefield simulation, was about 0.7 MPa when the Oita earthquake was triggered, with the static stress change being an order of magnitude smaller. The dynamic stress changes likely played an important role in triggering. A return to low seismicity levels 1 month after the triggered earthquake may have important implications for seismic hazard due to dynamic triggering.

Keywords: 2016 Kumamoto earthquake, Remote triggering, Coulomb failure stress change, Wavefield simulation

Background

Recent seismic observations have revealed that a single earthquake sometimes comprises slip on multiple faults. The 2009 Mw 8.1 Samoa–Tonga earthquake consisted of multiple large events in the outer rise region and on the megathrust (Beavan et al. 2010; Lay et al. 2010). The 2011 Mw 7.1 Araucania earthquake consisted of two events: a Mw 6.8 thrust event followed 12 s later by a Mw 6.7 event with a normal faulting mechanism and 30 km shallower (Hicks and Rietbrock 2015). The 2011 Mw 6.6 Fukushima earthquake occurred on two subparallel normal faults, where the rupture propagated from one fault to the other (Tanaka et al. 2014). The 2012 M8.6 East Indian Ocean earthquake occurred on multiple planes in an orthogonal conjugate fault system (e.g., Yue et al. 2012). The 2012 Mw 7.3 Sanriku-Oki earthquake occurred in the outer rise region, where a shallower Mw 7.2 normal faulting event was preceded by an Mw 7.1 reverse faulting earthquake about 22 s beforehand (Harada et al. 2013). The slip on the secondary fault in each case seems to result from either static triggering processes driven by permanent fault displacements near the source region (Harada et al. 2013), dynamic triggering processes by transient stress perturbations due to the passage of large seismic waves (Hicks and Rietbrock 2015), or a combination of the two processes (Tanaka et al. 2014). In general, both static and dynamic stress transfers play important roles in triggering slip on the secondary fault plane when the plane is located within one rupture length of the initially ruptured fault.

The Mw 7.0 Kumamoto earthquake of April 16, 2016, was accompanied ~30 s later by an M ~6 earthquake in central Oita prefecture, 80 km northeast of the hypocenter of the Kumamoto earthquake. Hereafter, this triggered earthquake is referred to as the "Oita

*Correspondence: miyazawa@rcep.dpri.kyoto-u.ac.jp
Disaster Prevention Research Institute, Kyoto University, Uji, Kyoto 611-0011, Japan

earthquake." It is well known that in geothermal regions, crustal materials are more sensitive to stress perturbations, and earthquakes are more easily triggered (e.g., Hill and Prejean 2015). In the case of the 2011 Mw 9.0 Tohoku-Oki earthquake, a few small earthquakes were remotely triggered in this area by passing surface waves (Miyazawa 2011; Fukui et al. 2012). Because the Kumamoto and Oita earthquakes were monitored by a dense seismic network, they were able to be distinguished. A triggered earthquake can be identified from observed waveforms near its epicenter (Fig. 1), peak ground motion (PGA) distributions (Fig. 2), and seismicity (Fig. 3). Figure 1 shows that the onset of the Oita earthquake occurred about 34 s after the origin time of the Kumamoto earthquake. Figure 2 shows the distribution of raw three-component PGA values recorded by the K-NET and KiK-net strong-motion networks and thought to be from the Kumamoto earthquake. The PGA values are the maximum amplitudes of the vector acceleration from the three components for a 100-s time window from the origin of the Kumamoto earthquake. The map was generated by smoothing these PGA values. There are two areas of peak PGA values (Fig. 2a), one of which (central Oita prefecture) disappears if the PGA values are calculated for the period prior to the arrival of waves from the Oita earthquake (Fig. 2b); thus, the secondary peak is mainly from the triggered earthquake. The magnitude of the Oita earthquake was tentatively estimated at 5.7 by the Japan Meteorological Agency (JMA), but this value was not well constrained because of overlapping waves from the Kumamoto earthquake. Earthquakes local to central Oita prefecture following the triggered earthquake are described as its aftershocks. Figure 3 shows seismicity for 15 days before and 2 months after the Kumamoto and Oita earthquakes. The seismicity rate in Oita decreased markedly within 1 month, despite the local aftershocks. No $M \geq 2.5$ earthquakes were observed during the next month.

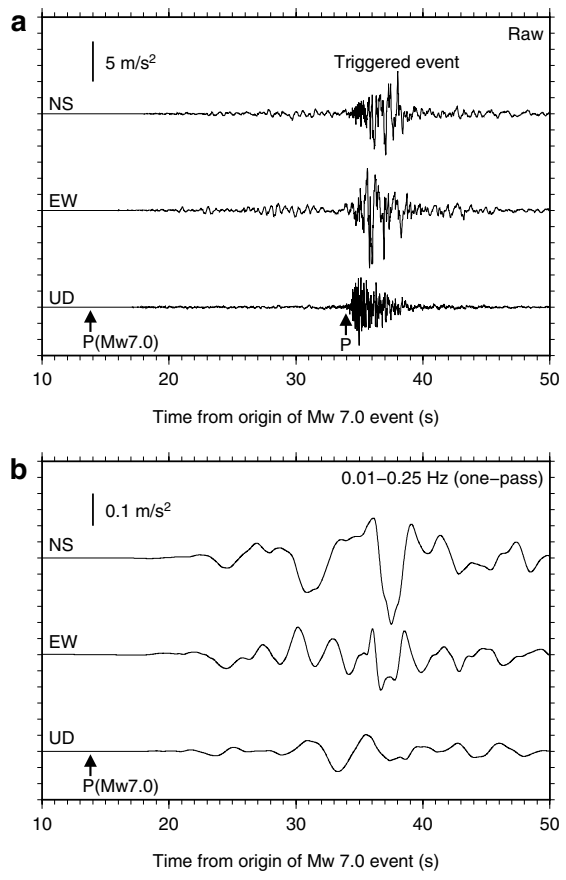

Fig. 1 Acceleration waveforms for the Mw 7.0 Kumamoto earthquake of April 16, 2016, recorded at K-NET station OIT009 (Yufuin). **a** Raw waveforms. **b** Waveforms band-pass-filtered between 0.01 and 0.25 Hz by use of a one-pass operation. *NS* north–south motion, *EW* east–west motion, and *UD* vertical motion (up–down). The arrivals of P waves from the Kumamoto and triggered earthquakes are indicated by *black arrows*. The station location is shown in Figs. 2a and 3a

The correlation between the triggering Kumamoto earthquake and the triggered Oita earthquake can be demonstrated by an integrated seismicity model (Miyazawa 2015), which statistically evaluates the time intervals between consecutive earthquakes. We modeled the seismicity using 30 shallow (depth $\leq$ 30 km) earthquakes with $M \geq 5.0$ since 1923 in the area of Fig. 3a and using the integrated seismicity model (more specifically, a stationary Poisson model) under the null hypothesis of no seismicity interaction between the Kumamoto and Oita earthquakes. The estimated probability that at least one earthquake of $M \geq 5.0$ occurs prior to the Oita earthquake and following the Kumamoto earthquake is only 3.3×10^{-5}%. This small value can reject the null hypothesis and statistically indicates that there may exist a causal relationship between the two consecutive events. Then, we need to investigate the physical process for this remote triggering.

It is noted that this two-earthquake sequence is the clearest known example of the remote triggering of a large ($M > \sim 6$) earthquake during the passage of seismic waves, whereas there were other examples reported previously (e.g., Lin 2012; Miyazawa 2015). The magnitudes of earthquakes triggered remotely by the passage of seismic waves are generally small ($M < \sim 4$) (e.g., Miyazawa et al. 2005; Miyazawa 2011; Peng et al. 2010; Yukutake et al. 2013). Thus, studying the Oita earthquake could advance our fundamental understanding of the triggering processes of large earthquakes.

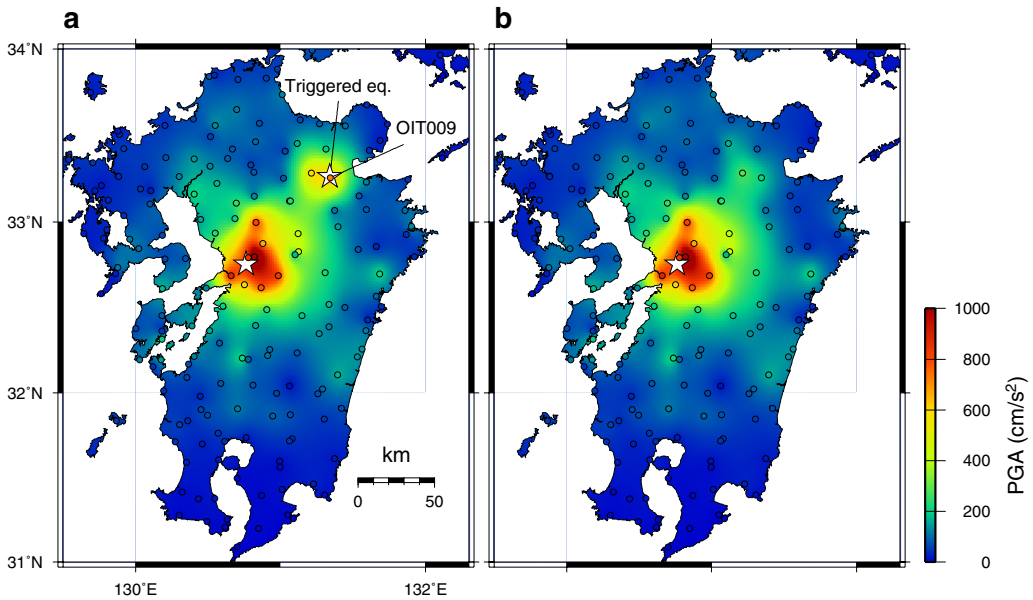

Fig. 2 Three-component PGA for the 2016 Kumamoto earthquake. **a** PGA map for the Kumamoto earthquake and the triggered Oita earthquake. **b** PGA map for the Kumamoto earthquake, excluding the triggered earthquake. PGA values were observed at K-net and KiK-net stations (*circles*), and the map was generated by smoothing these values. *White stars* represent the epicenters of the Kumamoto earthquake and (in 2a only) the triggered earthquake

Location of the triggered Oita earthquake and estimation of its mechanism

Because the first arrivals of the Oita earthquake were masked by high-amplitude seismic waves, its hypocenter has not yet been precisely estimated. Therefore, we begin by determining the location and magnitude of the Oita earthquake. A hypocenter is obtained using the program hypomh (Hirata and Matsu'ura 1987), using seismograms from permanent K-NET and KiK-net stations (Fig. 3a) and the JMA2001 velocity model (Ueno et al. 2002). To calculate a local magnitude, we use the largest amplitude of the envelope of the vertical velocity waveform, excluding the amplitude immediately before the P arrival to avoid overestimation.

The hypocenter of the Oita earthquake was located at a depth of 8.5 km beneath the Yufuin geothermal field, almost under station OIT009 (Fig. 3; Table 1). The origin time of the Oita earthquake was 32.5 s after that of the triggering Kumamoto earthquake, and its local magnitude was estimated at 5.9. Because the high-amplitude waves from the Kumamoto mainshock hinder the accurate picking of P and S arrivals, the location includes greater implicit errors than those listed in Table 1. The magnitude is obtained using amplitude data from only two stations near the hypocenter and therefore also has a high uncertainty. The hypocenter and magnitude are consistent with those obtained by other studies (e.g., Nakamura and Aoi 2016; Uchide et al. 2016; Yoshida 2016), where the hypocenters are located within an error range of ~1 km using different velocity models, and the moment magnitude or local magnitude ranges from 5.6 to 6.5.

A source model for the Oita earthquake is required to resolve temporal stress changes on the fault plane. However, such a source model is not available because of the overlapping waves from the Kumamoto earthquake. Even with the recorded displacements and waveforms at Yufuin, on the basis of a crude rupture size estimate from the magnitude, it is difficult to determine the mechanism and magnitude more precisely because the stations that clearly recorded the Oita earthquake were located very close to the rupture. Therefore, we can neither assume a double-couple source nor constrain the free parameters of the source fault.

The source mechanism of the largest aftershock of the Oita earthquake (M5.4/Mw 5.1, Fig. 3) and the displacements recorded at a global navigation satellite system (GNSS) site on the date of the Oita earthquake are helpful for this purpose. The centroid moment tensor (CMT) solution determined by JMA for the Mw 5.1 aftershock has strike, dip, and rake angles of N243°E, 68°, and −148°, respectively. We assume that the fault of the Oita earthquake strikes WSW–ENE, based on seismicity distributions and mapped fault segments in central Oita (National Institute of Advanced Industrial Science and Technology 2016). The horizontal and vertical displacements at the

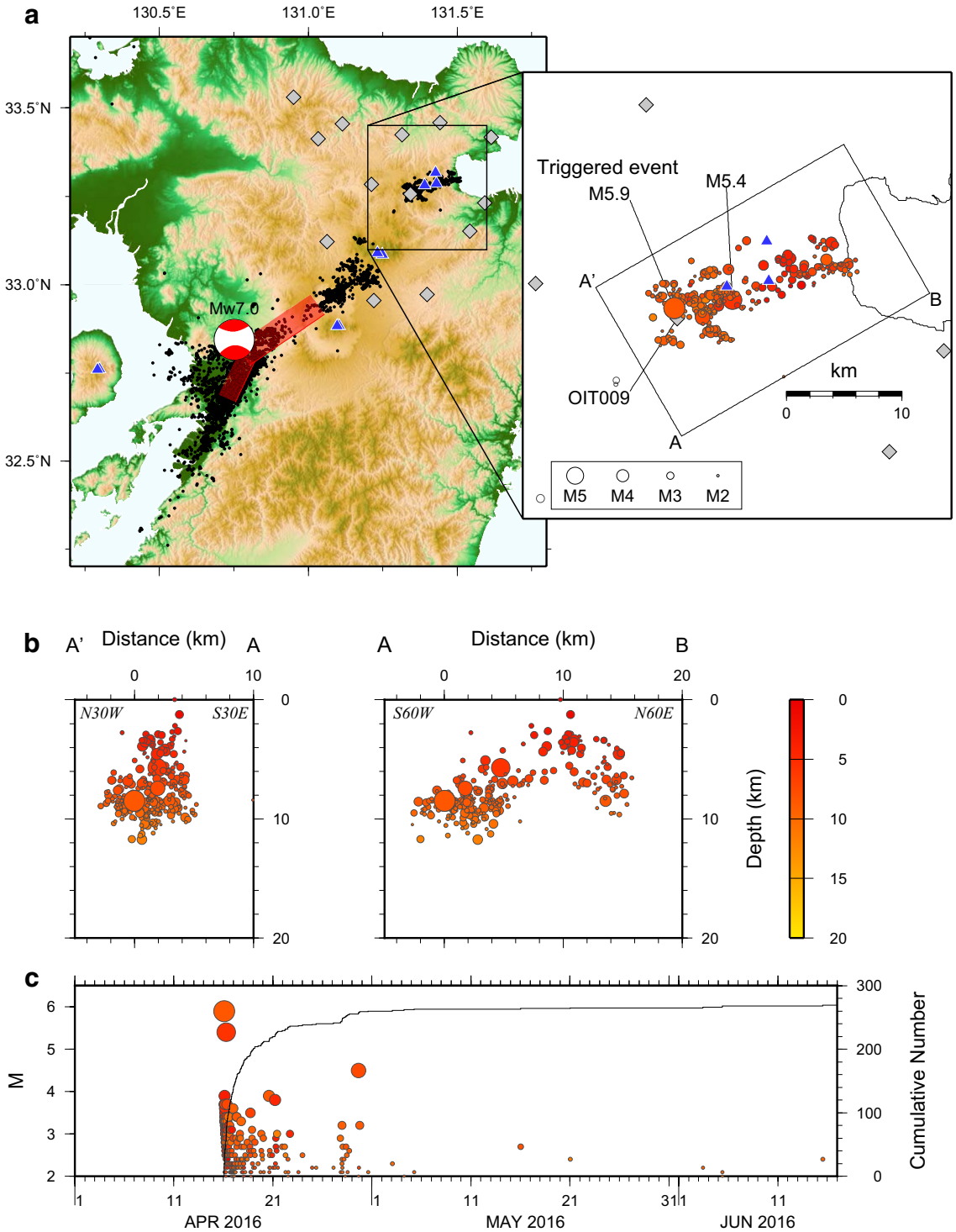

Fig. 3 Locations of $M \geq 2.0$ earthquakes at depths from 0 to 30 km for 15 days before and 2 months after the April 16, 2016, Mw 7.0 Kumamoto earthquake. **a** Left window shows the JMA CMT for the Kumamoto earthquake, other earthquakes (including foreshocks and aftershocks) from the JMA catalog (*solid circles*), and K-NET and KiK-net stations (*diamonds*) used to locate the Oita earthquake. The *rectangular* fault plane model of the Kumamoto earthquake by Asano and Iwata (2016) is shown in *red*. Active volcanoes are shown by *blue triangles*. The region of Oita prefecture outlined by the *black square* is magnified in the *inset*. The *color scale* is shown in (**b**). **b** Projections of hypocenters onto two orthogonal vertical planes in the right window of **a**. **c** Magnitude–time diagram of seismicity. The cumulative earthquake number is shown by a *solid line*

Table 1 Parameters of the large, triggered Oita earthquake

Origin time	Longitude (error)	Latitude (error)	Depth (error)	Magnitude
April 16, 2016 01:25:38.0 (UTC+9)	131.341°E (0.26)	33.2653°N (0.28)	8.47 km (0.42)	5.9

Values in brackets show location error estimates in km

GNSS site, which is located 0.5 km from OIT009, show 4.2 cm easting, 2.5 cm northing, and 5.5 cm subsidence on April 16 (UTC+9) (Geospatial Information Authority of Japan 2016). The observed subsidence is mainly due to the Oita earthquake. The horizontal displacements are also probably due to this earthquake, but might be partly due to the Kumamoto earthquake. Taking these observations into account, we assume that the Oita earthquake has strike N240°E, dip 70°, and rake −140°.

Triggering stress changes from the 2016 Kumamoto earthquake

We estimate the stress change in the Oita earthquake's source region due to the Kumamoto earthquake. Previous studies of remote triggering have approached this problem either by forward techniques with simple layered models (e.g., Rubinstein et al. 2007; Hill 2012) or by inverse approaches using observed waveforms via transport kernels (e.g., Miyazawa and Brodsky 2008; Miyazawa 2015). However, both of those approaches model surface waves. In the present case, such approaches might be inapplicable because it is not clear whether body or surface wave phases triggered the Oita earthquake. To reproduce the observed waveforms and estimate the stress changes at depth, we use SEISM numerical modeling software for elastic wave simulation (e.g., Maeda and Furumura 2013; Maeda et al. 2013), with the Japan Integrated Velocity Structure Model (Koketsu et al. 2012) for the three-dimensional structure. This approach solves the equations of motion in three-dimensional Cartesian coordinates with viscoelastic constitutive equations, using a finite difference method to fourth order in space and second order in time. The spatial grid size is 0.5 km in the horizontal and vertical directions, and the time step is 0.025 s. For the source model of the Kumamoto earthquake, we use the JMA CMT solution (Fig. 3). The advantages of the numerical method include (1) time-dependent changes associated with the far-field and near-field terms are simultaneously considered, and (2) changes in the stress tensor at depth are directly available, even in a heterogeneous three-dimensional structure.

Figure 4 shows recorded and simulated velocity waveforms at station OIT009 from the 2016 Kumamoto earthquake by using the SEISM program. Note that the times of the simulated waves were delayed by 3.0 s to maximize the correlation between observed and synthetic data before the Oita earthquake. This delay was necessary because we assumed a point source for the Kumamoto earthquake, whereas the CMT solution was obtained from waveforms at periods of 45–200 s, and slip distribution on the fault plane was not taken into consideration. A similar time delay needed to be imposed at other nearby stations too. Simulated waveforms are generally consistent with recorded data for the low-frequency components in Fig. 4, though the filtered waveforms are strongly influenced by overlapping waves from the Oita earthquake, and a point-source approximation is reasonable in the present study. Small higher-frequency components cannot be meaningfully simulated, because the fine-scale structures and high-frequency source-time function are not modeled here. The low-amplitude vertical component first arrivals seem to show an anti-phase relationship between observations and simulations, although this is because the station is located at the extension of a nodal plane of the Kumamoto earthquake (Fig. 3), and the vertical component is considerably sensitive to the strike direction, making it difficult to match the sense of the first motion without introducing ad hoc constraints to the waveform modeling process.

We then resolve temporal stress changes on the fault plane of the Oita earthquake. The source mechanism of the Oita earthquake is roughly estimated in the previous section, but estimates of those fault parameters must consider uncertainties, so we calculate the stress changes by varying the fault strike from N220°E to N260°E, the dip from 60° to 80°, and the rake from −160° to −120°. Finally, we estimate the change in the Coulomb failure stress at the hypocenter, as given by

$$\Delta \mathrm{CFF} = \Delta\tau + \mu' \Delta\sigma_n, \tag{1}$$

where the effective friction coefficient μ' is assumed to be 0.4 and $\Delta\tau$ and $\Delta\sigma_n$ are the shear stress change in the slip direction and the normal stress change on the fault plane (negative for compression), respectively. The Lamé parameters, λ and μ, are each set to 30 GPa.

The changes in Coulomb failure stress at the hypocenter of the Oita earthquake, using the assumed mechanism referred to above and the simulated waveform data, are shown in Fig. 5a. Changing the hypocenter location does not result in significant differences relative to

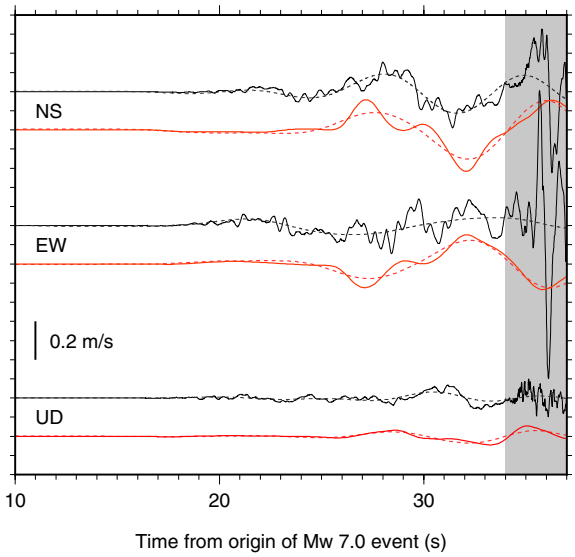

Fig. 4 Recorded and simulated waveforms at OIT009. *NS* north–south, *EW* east–west, *UD* up–down components, respectively. Recorded waveforms are in *black*, simulated waveforms are in *red*, unfiltered data are shown with *solid lines*, and filtered data (0.05–0.20 Hz) are shown with *broken lines*. The time window of the Oita earthquake is *shaded*

mechanism errors. The triggering ΔCFF at the origin time is about 650 kPa near the waveform peak and varies from 80 to 780 kPa when accounting for uncertainty in the mechanism. A source model with a higher value of 780 kPa has a steeper dip and a lower rake compared with the reference model (i.e., close to a right-lateral strike-slip fault), whereas a model with a lower value has a mechanism close to normal faulting. The static stress change, the ΔCFF value 1000 s after the origin time of the Kumamoto earthquake, is 21 kPa and varies from 5 to 25 kPa when uncertainties in the mechanism are taken into account. All of these values are positive to promote slip on the fault plane, and all are larger than the expected tidal stress change of about 10 kPa. The values of the dynamic stress changes are about one order of magnitude greater than the corresponding static stress change values, suggesting that dynamic stress changes likely play an important role in triggering.

Figure 5b shows the volumetric strain changes at the hypocenter, the values of which are independent of the uncertainties in the triggered source mechanism. The triggering strain change varies about from 4×10^{-7} to 7×10^{-7}, and the corresponding static strain change is about 1×10^{-7}. Because the Oita earthquake was not triggered by the preceding peak strains, which exceeded the strain at the origin time, it is inferred that the volumetric strain change was not the only important parameter in the triggering process.

Discussion

Assuming that the source of the Oita earthquake is similar to that in the reference model and that the stress changes caused by the Mw 7.0 Kumamoto earthquake contributed to the occurrence of the Oita earthquake, the following scenario may describe the physical process of triggering. Frictional stress transiently increased by about 0.7 MPa because of the Kumamoto earthquake, about one order of magnitude less than the stress drop of a typical earthquake, but enough to exceed the frictional strength required to trigger an earthquake on the generating fault. The large transient stress change required for triggering may suggest that the background stress difference was relatively low. On the other hand, this fault was closer to failure than other faults in this region, because there were no triggered earthquakes on the other faults. Although the relationship between triggering stress and triggered event magnitude has been thoroughly investigated only for tectonic tremors (e.g., Miyazawa and Mori 2006; Miyazawa and Brodsky 2008), there have been case studies that suggest earthquakes of $M > 4$ can be triggered by large transient stress changes. For example, the 2011 Mw 9.0 Tohoku-Oki earthquake remotely and dynamically triggered M ~4 earthquakes at Hakone volcano, Japan, with triggering stresses of ~100 kPa, a location where no earthquake of $M > 4.0$ had been recorded since 1995 (Yukutake et al. 2011, 2013). In the present case, too, large stress changes on the fault are thought to have directly triggered the large earthquake. Parsons et al. (2012) used simulated wavefields to show that dynamic stress changes from surface waves rarely trigger $M > 5$ earthquakes and concluded that there is an inconsistency between target fault rake and imposed stress change direction and that the window in which the dynamic stress field change favors triggering is temporally short and spatially small. In the present case, because the rake of the imposed slip matched the rake of the triggered fault, and because the resolved triggering stress was sufficiently large, it might have been easy for a rupture to propagate in the favorable direction. Stress transfer from the Oita earthquake then triggered aftershocks to an extent, but seismicity abruptly returned to background levels within a month. Since aftershocks are in general triggered by stress changes caused by the mainshock, this may indicate that the static stress changes caused by the Oita earthquake could not have remarkably exceeded the triggering threshold with a low background stress difference. These observations suggest the following: (1) The fault of the Oita earthquake was not originally close to failure at the time of the Kumamoto earthquake, but the large transient stress changes from the Kumamoto earthquake triggered the Oita earthquake and/or (2) the apparent quiescence of aftershocks following the Oita

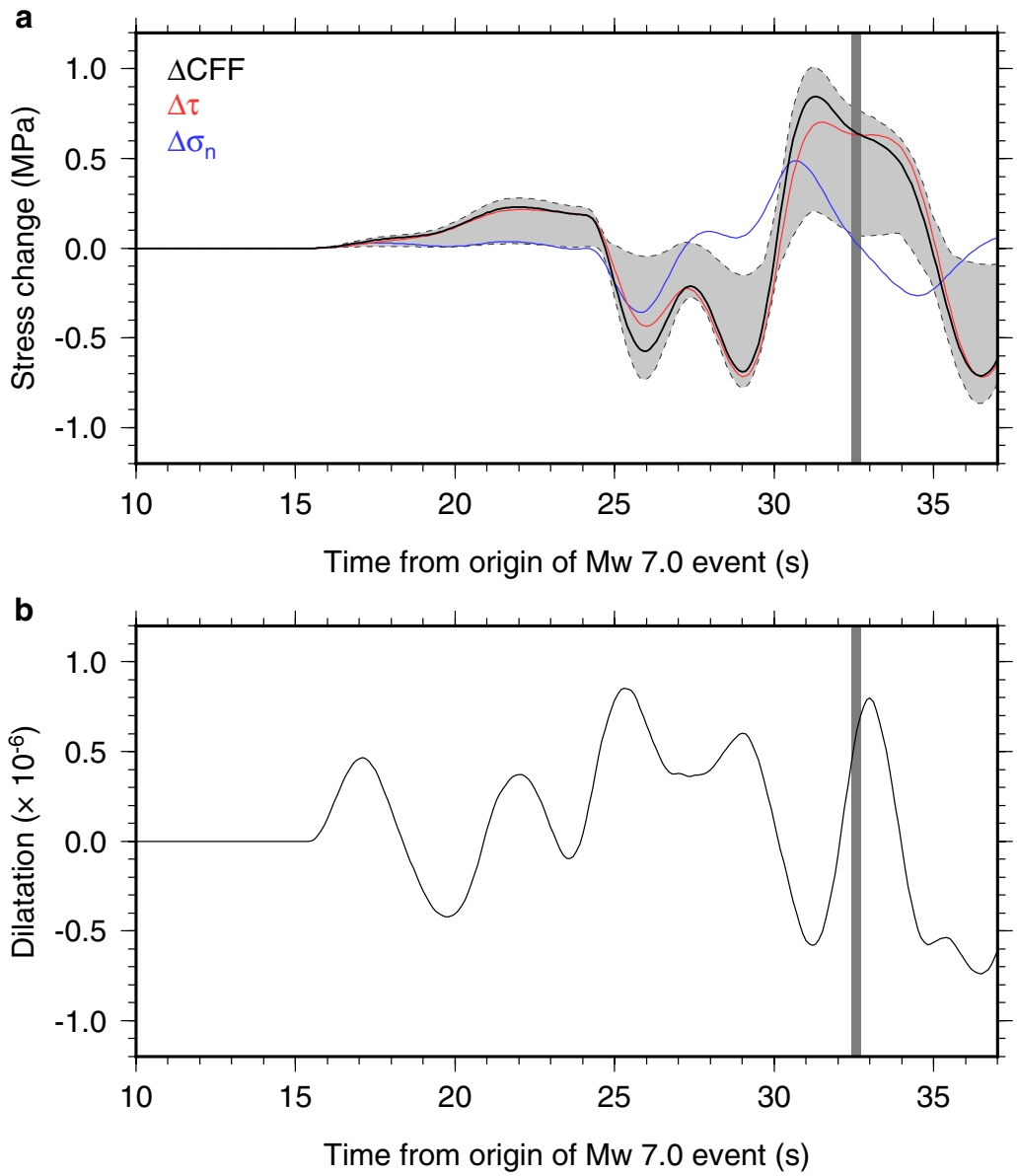

Fig. 5 Changes in stress and volumetric strain (dilatation) at the hypocenter of the Oita earthquake. **a** Changes in the Coulomb failure stress (ΔCFF), shear stress ($\Delta\tau$), and normal stress ($\Delta\sigma_n$) are shown in *black*, *red*, and *blue lines*, respectively. The *shaded* region indicates variability of ΔCFF due to changes in the mechanism of the Oita earthquake (see text for full procedural description). The *gray bar* indicates the origin time of the Oita earthquake. **b** Volumetric strain changes at the hypocenter. Positive values indicate expansion

earthquake is temporary, and eventually there will be significant seismicity.

Conclusions

This study used a full wavefield simulation to investigate the triggering process of the M5.9 Oita earthquake, which was remotely triggered by passing seismic waves from the Mw 7.0 Kumamoto earthquake of April 16, 2016. At the hypocenter of the Oita earthquake, the change in Coulomb failure stress increased by as much as 0.7 MPa at the origin time and likely played an important role in triggering. Taking the scarcity of the aftershocks of the Oita earthquake into consideration, the generating fault might not have been close to failure before the Kumamoto earthquake; alternatively, there may eventually be significant seismicity.

Acknowledgements
We used the seismicity catalog of the Japan Meteorological Agency (JMA). Seismic waveform data are from K-NET and KiK-net stations operated by the National Research Institute for Earth Science and Disaster Resilience (NIED), Japan. Plots were made using the Generic Mapping Tools (Wessel and Smith 1998). For data analysis, we used the computer systems of the Earthquake and Volcano Information Center of the Earthquake Research Institute (ERI), University of Tokyo, Japan. This study was partially supported by ERI under Joint Usage Research Project (B) 2015-B-01. We thank Dr. Hector Gonzalez-Huizar and an anonymous reviewer for careful and thoughtful reviews.

Competing interests
The author declares that he has no competing interests.

Received: 21 July 2016 Accepted: 6 December 2016
Published online: 19 December 2016

References

Asano K, Iwata T (2016) Source rupture processes of the foreshock and mainshock in the 2016 Kumamoto earthquake sequence estimated from the kinematic waveform inversion of strong motion data. Earth Planets Space 68:147. doi:10.1186/s40623-016-0519-9

Beavan J, Wang X, Holden C, Wilson K, Power W, Prasetya G, Bevis M, Kautoke R (2010) Near-simultaneous great earthquakes at Tongan megathrust and outer rise in September 2009. Nature 466:959–964. doi:10.1038/nature09292

Fukui M, Kobayashi R, Goto K (2012) Dynamic triggering of earthquakes in Kyushu during the passage of seismic waves from the 2011 off the Pacific coast of Tohoku earthquake. Rep Fac Sci 45:31–41

Geospatial Information Authority of Japan (2016) Crustal deformation associated with the 2016 Kumamoto earthquake. http://www.gsi.go.jp/chibankansi/chikakukansi_kumamoto20160414.html. Accessed 17 Jun 2016

Harada T, Murotani S, Satake K (2013) A deep outer-rise reverse-fault earthquake immediately triggered a shallow normal-fault earthquake: the 7 December 2012 off-Sanriku earthquake (Mw 7.3). Geophys Res Lett 40:4214–4219. doi:10.1002/grl.50808

Hicks SP, Rietbrock A (2015) Seismic slip on an upper-plate normal fault during a large subduction megathrust rupture. Nat Geosci 8:955–960. doi:10.1038/ngeo2585

Hill DP (2012) Dynamic stresses, coulomb failure, and remote triggering—corrected. Bull Seism Soc Am 102:2313–2336. doi:10.1785/0120120085

Hill D, Prejean S (2015) Dynamic triggering. In: Kanamori H (ed) Earthquake seismology. Treatise on geophysics, vol 4, 2nd edn. Elsevier, Amsterdam, pp 273–304. doi:10.1016/B978-0-444-53802-4.00078-6

Hirata N, Matsu'ura M (1987) Maximum-likelihood estimation of hypocenter with origin time eliminated using nonlinear inversion technique. Phys Earth Planet Inter 47:50–61. doi:10.1016/0031-9201(87)90066-5

Koketsu K, Miyake H, Suzuki H (2012) Japan integrated velocity structure model version 1. In: Proceedings of the 15th world conference on earthquake engineering, Lisbon, Portugal

Lay T, Ammon CJ, Kanamori H, Rivera L, Koper KD, Hutko AR (2010) The 2009 Samoa-Tonga great earthquake triggered doublet. Nature 466:964–968. doi:10.1038/nature09214

Lin CH (2012) Remote triggering of the Mw 6.9 Hokkaido Earthquake as a result of the Mw 6.6 Indonesian earthquake on September 11, 2008. Terr Atmos Ocean Sci 23:283–290. doi:10.3319/TAO.2012.01.12.01(T)

Maeda T, Furumura T (2013) FDM simulation of seismic waves, ocean acoustic waves, and tsunamis based on tsunami-coupled equations of motion. Pure appl Geophys 170:109–127. doi:10.1007/s00024-011-0430-z

Maeda T, Furumura T, Noguchi S, Takemura S, Sakai S, Shinohara M, Iwai K, Lee SJ (2013) Seismic and tsunami wave propagation of the 2011 Off the Pacific Coast of Tohoku Earthquake as inferred from the tsunami-coupled finite difference simulation. Bull Seism Soc Am 103:1456–1472. doi:10.1785/0120120118

Miyazawa M (2011) Propagation of an earthquake triggering front from the 2011 Tohoku-Oki earthquake. Geophys Res Lett 38:L23307. doi:10.1029/2011GL049795

Miyazawa M (2015) Seismic fatigue failure may have triggered the 2014 Mw7.9 Rat Islands earthquake. Geophys Res Lett 42:2196–2203. doi:10.1002/2015GL063036

Miyazawa M, Brodsky EE (2008) Deep low-frequency tremor that correlates with passing surface waves. J Geophys Res 113:B01307. doi:10.1029/2006JB004890

Miyazawa M, Mori J (2006) Detection of triggered deep low-frequency events from the 2003 Tokachi-oki earthquake. Geophys Res Lett 32:L10307. doi:10.1029/2005GL022539

Miyazawa M, Nakanishi I, Sudo Y, Ohkura T (2005) Dynamic response of frequent tremors at Aso volcano to teleseismic waves from the 1999 Chi-Chi, Taiwan earthquake. J Volcanol Geotherm Res 147:173–186. doi:10.1016/j.jvolgeores.2005.03.012

Nakamura T, Aoi S (2016) Source location and mechanism analysis of an earthquake triggered by the 2016 Kumamoto, southwestern Japan, earthquake. Earth Planets Space. doi:10.1186/s40623-016-0588-9

National Institute of Advanced Industrial Science and Technology (2016) Active fault database of Japan. https://gbank.gsj.jp/activefault/index_e_gmap.html. Accessed 4 May 2016

Parsons T, Kaven JO, Velasco AA, Gonzalez-Huizar H (2012) Unraveling the apparent magnitude threshold of remote earthquake triggering using full wavefield surface wave simulation. Geochem Geophys Geosyst 13:Q06016. doi:10.1029/2012GC004164

Peng Z, Wang W, Chen QF, Jiang T (2010) Remotely triggered seismicity in north China following the 2008 Mw 7.9 Wenchuan earthquake. Earth Planets Space 62:893–898. doi:10.5047/eps.2009.03.006

Rubinstein JL, Vidale JE, Gomberg J, Bodin P, Creager KC, Malone SD (2007) Non-volcanic tremor driven by large transient shear stresses. Nature 448:579–582. doi:10.1038/nature06017

Tanaka M, Asano K, Iwata T, Kubo H (2014) Source rupture process of the 2011 Fukushima-ken Hamadori earthquake: how did the two subparallel faults rupture? Earth Planets Space 66:101. doi:10.1186/1880-5981-66-101

Uchide T, Horikawa H, Nakai M, Matsushita R, Shigematsu N, Ando R, Imanishi K (2016) The 2016 Kumamoto-Oita earthquake sequence: aftershock seismicity gap and dynamic triggering in volcanic areas. Earth Planets Space 68:180. doi:10.1186/s40623-016-0556-4

Ueno H, Hatakeyama S, Aketagawa T, Funasaki J, Hamada N (2002) Improvement of hypocenter determination procedures in the Japan Meteorological Agency. Quart J Seismol 65:123–134

Wessel P, Smith WHF (1998) New, improved version of generic mapping tools released. EOS Trans Am Geophys Union 79:579. doi:10.1029/98EO00426

Yoshida S (2016) Earthquakes in Oita triggered by the 2016 M7.3 Kumamoto earthquake. Earth Planets Space 68:176. doi:10.1186/s40623-016-0552-8

Yue H, Lay T, Koper K (2012) En echelon and orthogonal fault ruptures of the 11 April 2012 great intraplate earthquakes. Nature 490:245–249. doi:10.1038/nature11492

Yukutake Y, Honda R, Harada M, Aketagawa T, Ito H, Yoshida A (2011) Remotely-triggered seismicity in the Hakone volcano following the 2011 off the Pacific coast of Tohoku earthquake. Earth Planets Space 63:737–740. doi:10.5047/eps.2011.05.004

Yukutake Y, Miyazawa M, Honda R, Harada M, Ito H, Sakaue M, Koketsu K, Yoshida A (2013) Remotely triggered seismic activity in Hakone volcano during and after the passage of surface waves from the 2011 M9.0 Tohoku-Oki earthquake. Earth Planet Sci Lett 373:205–216. doi:10.1016/j.epsl.2013.05.004